

Laser ablation of silicon induced by a femtosecond optical vortex beam

JIJIL JJ NIVAS,^{1,2} HE SHUTONG,^{1,3} ANOOP K.K.,^{1,2} A. RUBANO,^{1,2} R. FITTIPALDI,⁴
A. VECCHIONE,⁴ D. PAPARO,² L. MARRUCCI,^{1,2} R. BRUZZESE,^{1,2} AND S.
AMORUSO^{1,2,*}

¹Dipartimento di Fisica, Università di Napoli Federico II, Complesso Universitario di Monte S. Angelo, Via Cintia, I-80126 Napoli, Italy

²CNR-SPIN UOS Napoli, Complesso Universitario di Monte S. Angelo, Via Cintia, I-80126 Napoli, Italy

³Ultrafast Laser Laboratory, Key Laboratory of Opto-electronic Information Technical Science of Ministry of Education, College of Precision Instruments and Opto-electronics Engineering, Tianjin University, Tianjin 300072, China

⁴CNR-SPIN, UOS Salerno, Via Giovanni Paolo II 132, I-84084 Fisciano, Italy

*Corresponding author: amoruso@na.infn.it

Received XX Month XXXX; revised XX Month, XXXX; accepted XX Month XXXX; posted XX Month XXXX (Doc. ID XXXXX); published XX Month XXXX

We investigate laser ablation of crystalline silicon induced by a femtosecond optical vortex beam, addressing how beam properties can be obtained by analyzing the ablation crater. The morphology of the surface structures formed in the annular crater surface allows direct visualization of the beam polarization, while analysis of crater size provides beam spot parameters. We also determined the diverse threshold fluences for the formation of various complex microstructures generated within the annular laser spot on the silicon sample. Our analysis indicates an incubation behavior of the threshold fluence as a function of the number of laser pulses, independently of the optical vortex polarization, in weak focusing conditions. © 2015 Optical Society of America

OCIS codes: (140.3295) Laser beam characterization; (320.2250) Femtosecond phenomena; (320.7130) Ultrafast processes in condensed matter, including semiconductors.

<http://dx.doi.org/10.1364/OL.99.099999>

Laser ablation with intense femtosecond (fs) pulses is a valuable tool in many applications, as for example direct surface structuring of solid targets [1, 2], generation of nanoparticles [3, 4], fabrication of nanostructured films by deposition of the ablation plume [5, 6], and so forth. In particular, direct fs laser surface processing attracts increasing interest as an effective way to fabricate surface structures at nano- and micro-scales on metals and semiconductors. It has demonstrated the creation of diverse kinds of structures with the ability to modify, for example, the optical and wetting properties of samples in a flexible, simple and controllable way. Typically, a fs laser beam with a Gaussian intensity profile is focused onto the surface of the solid target under study. The focal length of the focusing lens is usually quite long generating a spot diameter of 10 μm or larger [1, 2]. Ablation occurs when the peak laser fluence is larger than the ablation threshold of the material. The properties of the ablation process are related to the beam characteristics and for laser beams with a Gaussian intensity profile are obtained by a well-established method based on the analysis of the

lateral dimensions of the crater produced on the target [7, 8]. In fact, crater analyses allow determining beam waist, peak fluence of the laser pulse, as well as the fluence threshold for ablation of the target material and the conditions for the formation of specific surface structures. All these parameters are fundamental for an accurate description of the experimental conditions and for a clear analysis of the investigated processes.

Recently, laser beams with non-Gaussian intensity profile are gaining attention as a novel prospect in laser-matter interaction, and related applications [9-11]. In particular, the current development of efficient beam converters generating powerful fs optical vortex pulses offers the possibility of observing new experimental aspects in this emerging topic [11-15]. The use of optical vortex (OV) beams in fs laser ablation and surface structuring has recently led to the generation of sub-wavelength ring structures on silicon or glass [12, 13], and production of surface micro-structures on stainless steel, silicon and copper [15-18]. These microstructures evidence a clear relationship with the spatial distribution of laser beam intensity and polarization.

Laser induced structures and crater profiles have been used as a direct way to diagnose intense, cylindrical vector beams in the focal plane [13-15, 19, 20, 21]. For example, Hnatosky et al. used the ablation craters produced in glass [19] and silicon [13] to evidence the generation of an intense longitudinal component of the electric field at the focus of fs laser beams produced in tight focusing conditions. Moreover, Toyoda et al. exploited chirality of micro-needles formed during nanosecond laser ablation to evidence the helicity of OV beams [20]. Recently, laser induced surface structures were also used to verify the state of polarization of fs OV beams at and around the focal plane [14-15, 21]. This, in turn, provides a simple and direct way to characterize the two-dimensional vector field structure of intense fs laser beams in weak focusing conditions, for which the longitudinal-component of the electric field is negligible [11, 21]. Actually, there is no research work addressing the optimal conditions for the formation of the diverse surface structures produced during laser irradiation of a solid target with a fs OV beam. Therefore, a detailed understanding of the diverse threshold fluences for ablation and for the formation of the various surface microstructures is essential to achieve an accurate and reliable determination of the OV beam properties.

Here, we report an analysis of crater and surface structures produced in direct fs laser ablation of silicon with an OV beam, demonstrating an effective method for characterizing the OV beam properties. Silicon is selected as a case study, being the most basic and studied semiconductor material widely applied in mechanical, optical and electronic devices. The optical vortex beam is generated via spin-to-orbital conversion of the angular momentum of light by using a q-plate [22, 23].

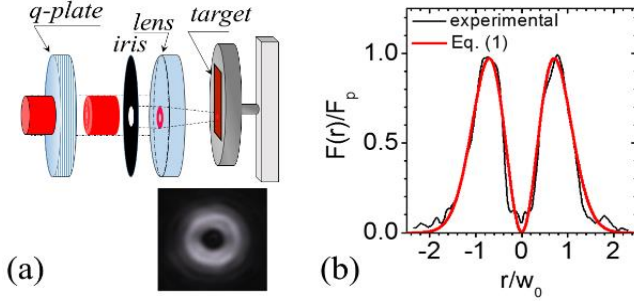


Fig. 1. (a) Schematic of the experimental setup. The inset shows the vortex beam spatial intensity profile. (b) Normalized spatial profile of the pulse fluence along the diameter of the beam (in units of the beam waist w_0).

Figure 1(a) reports a schematic of the experimental setup. The laser source is a Ti:Sa laser system delivering linearly polarized ≈ 35 fs pulses at 800 nm. An OV beam, carrying an orbital angular momentum (OAM) $\ell = \pm 1$, is produced by a q-plate with a topological charge $q = 1/2$. The inset in Fig. 1(a) reports an image of the beam spatial intensity distribution as acquired by a beam profiler. It is characterized by an annular spatial profile, with a central region of zero intensity due to an undefined phase on the OV beam axis. Fig. 1(b) shows the normalized intensity variation of the fluence along a diameter. Direct fs laser ablation of silicon (100) was induced by focusing the OV beam on the target surface with a lens of 75 mm focal length, in air. The target was mounted on a XY-translation stage located perpendicular to the laser beam direction (Figure 1(a)). An electromechanical shutter provided the selection of the desired number of laser pulses, N , applied to the same spot on the target. The morphology of the irradiated surface was analyzed by a scanning electron microscope (FESEM, model Zeiss Sigma).

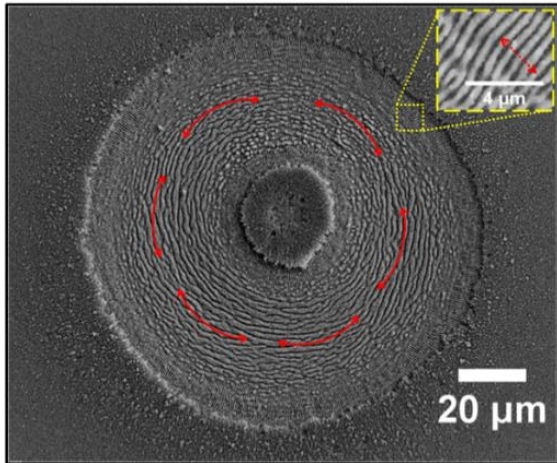


Fig.2. SEM micrograph of the target surface after irradiation with an azimuthally polarized OV beam at an energy $E_0 \approx 30 \mu\text{J}$, after $N = 100$ laser pulses. The red arrows indicate the laser beam polarization. The inset shows the morphology of the ripples formed in the outer region of the beam spot.

Fig. 2 reports an example of a typical SEM micrograph of the silicon surface irradiated area for $N=100$, for an azimuthal polarization. It shows the formation of a shallow, annular crater reflecting the beam shape. A complex surface morphology is observed in Fig. 2, with various annular regions characterized by different surface textures. The central region with a radius $R_{in} \approx 12 \mu\text{m}$ is decorated by a large number of nanoparticles, and corresponds to the central part of the beam with intensity well below the target ablation threshold. The external circle of the ablated area has a radius $R_{ex} \approx 58 \mu\text{m}$ and marks the transition to a fluence lower than the ablation threshold. The region just beyond R_{ex} is also densely decorated by nanoparticles. The ablated crater defined by the annulus going from R_{in} to R_{ex} , presents an inner region with a width of $\approx 25 \mu\text{m}$ characterized by micro-wrinkles aligned along the beam polarization, surrounded by two adjacent areas where subwavelength ripples are aligned perpendicular to the laser polarization. The inset of Fig. 2 shows a zoomed view of these ripples. The radial widths of these two areas are $\approx 7 \mu\text{m}$ (inner) and $\approx 12 \mu\text{m}$ (outer), respectively. The diverse width of these two regions is likely due to the different fluence spatial gradient in the central ($r < r_p$) and outer ($r > r_p$) regions of the OV beam profile (see Figure 1(b)).

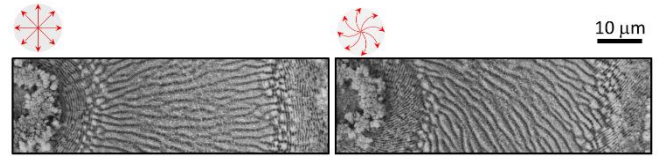


Fig. 3. Zoomed views of a portion of the ablation crater for radial (left panel) and spiral (right panel) polarization of the OV beam, at $E_0 = 50 \mu\text{J}$ and $N = 100$. The red arrows sketch the state of polarization.

The polarization of the OV beam can be appropriately changed by varying the angle between the linear polarization of the input Gaussian beam and the q-plate axis, which eventually affects the surface structure morphology. As an example, Fig. 3 reports two SEM micrographs of the silicon surface after irradiation with radially and spirally polarized OV beams, at $N=100$ and $E_0 = 50 \mu\text{J}$. The radial and spiral polarization were obtained by rotating the input polarization by an angle $\Delta\theta = 90^\circ$ and $\Delta\theta = 45^\circ$, respectively, with respect to the azimuthal case. Other patterns were also generated either by varying the value of $\Delta\theta$ or by using quarter-waveplates. In all cases, micro-wrinkles aligned along the local beam polarization are present in the higher fluence region, while ripples perpendicular to the polarization are formed in the low fluence areas. This, in turn, suggests a deterministic relationship between orientation and characteristic size of the surface structure and local polarization and fluence of the OV beam. Moreover, clear threshold fluences exist for ripples formation and for the sharp transition from ripples to wrinkles, which occurs at given locations within the ablation crater. We also observe that varying the laser pulse energy or number of pulses change the proportion between regions where ripples and micro-wrinkles appear. It is worth noting that earlier studies mainly focused on subwavelength ripples [1, 2, 8, 9, 14-16, 21], while more detailed analyses of micro-wrinkles produced by fs Gaussian beams started only very recently [24, 25]. Our findings indicate that the two structures are ubiquitous to fs laser ablation of silicon. Hence, we investigated the threshold fluence for the formation of both structures and how it depends on the OV beam properties.

The spatial profile of the pulse fluence $F(r)$, along the diameter of an OV beam with $\ell = \pm 1$, as a function of the radial coordinate r is described by the following distribution [11]:

$$F(r) = 2^2 E_0 \frac{r^2}{\pi w_0^4} e^{-\frac{2r^2}{w_0^2}} \quad (1)$$

where E_0 is the beam energy and w_0 the waist of the corresponding fundamental Gaussian beam. Eq(1) well approximates the experimental profile as shown in Fig. 1(b). The spatial distribution in Fig. 1(b) shows the presence of a null fluence at the beam center, and of two symmetric peaks at the positions $\pm r_p$, where r_p is given by:

$$r_p = \frac{w_0}{\sqrt{2}} \quad (2)$$

The corresponding peak fluence value F_p is:

$$F_p = F(r_p) = 2e^{-1} \frac{E_0}{\pi w_0^2} \approx 0.736 \frac{E_0}{\pi w_0^2} \quad (3)$$

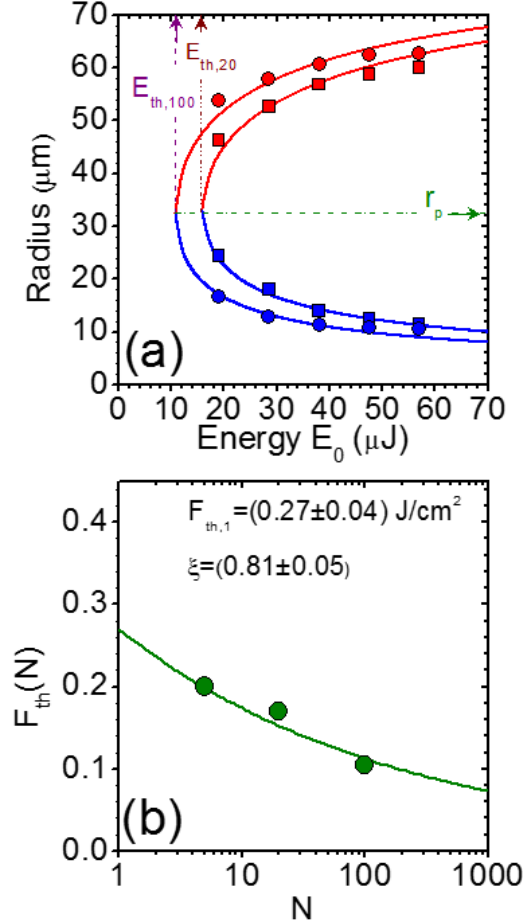


Fig. 4. (a) Examples of the variation of the internal (R_{in} , blue data points) and external (R_{ex} , red data points) radii as a function of the OV beam energy E_0 for two different number of pulses N : squares - $N=20$, circles - $N=100$. (b) Variation of the fluence threshold F_{th} with the number of pulses N . The uncertainties on the experimental data points are contained within their respective size. The line is a fit to the dependence $F_{th,N} = F_{th,1} \times N^{\xi-1}$ with the values of the fitting parameters shown in the figure.

We discuss first the variation of the internal, R_{in} , and external, R_{ex} , radii as a function of the OV laser pulse energy E_0 . R_{in} and R_{ex} marks the threshold for ablation and ripples formation. Fig. 4 reports two examples of the experimental dependence of R_{in} and R_{ex} as a function of E_0 , for $N=20$, and $N=100$, in the case of irradiation with an azimuthally polarized OV beam. One can observe a progressive reduction of the width of the ablated annulus ($R_{ex}-R_{in}$) as the energy E_0 decreases. This annulus eventually degenerates into a limiting circumference with a radius $R_{in}=R_{ex}=r_p$ when E_0 reaches the threshold level E_{th} , and the peak fluence F_p corresponds to the threshold fluence F_{th} , i.e.:

$$F_{th} = 2e^{-1} \frac{E_{th}}{\pi w_0^2} \quad (4)$$

The variation of R_{in} and R_{ex} vs E_0 can be modeled by solving the equation $F(r) = F_{th}$. An analytical solution for this equation does not exist. However, fits to the experimental data can be obtained through a numerical resolution coupled to a minimization procedure, and are reported as solid curves in Fig. 4(a). The experimental data are well described by the two branches departing from the point of coordinates (E_{th}, r_p) , and corresponding to R_{in} and R_{ex} vs E_0 . The beam waist w_0 and the threshold fluence F_{th} were used as fitting parameters, thus obtaining $w_0 = (46 \pm 2) \mu\text{m}$, and the values of the threshold fluence F_{th} reported in Fig. 4(b) for three different N values. We observe a progressive reduction of F_{th} with N , similarly to what reported earlier for the case of fs laser ablation of silicon with fs laser pulses characterized by a Gaussian intensity spatial profile [8]. This trend was observed for different materials, and is explained as an incubation behavior described by the dependence $F_{th,N} = F_{th,1} \times N^{\xi-1}$, where ξ is a material-dependent incubation factor ($\xi = 0.84$ was reported for silicon [8]). The solid line in Fig. 4(b) is a fit to the incubation dependence, yielding $F_{th,1} = (0.27 \pm 0.04) \text{ J/cm}^2$ and $\xi = (0.81 \pm 0.05)$, consistent with the previous results of Bonse et al. for silicon [8].

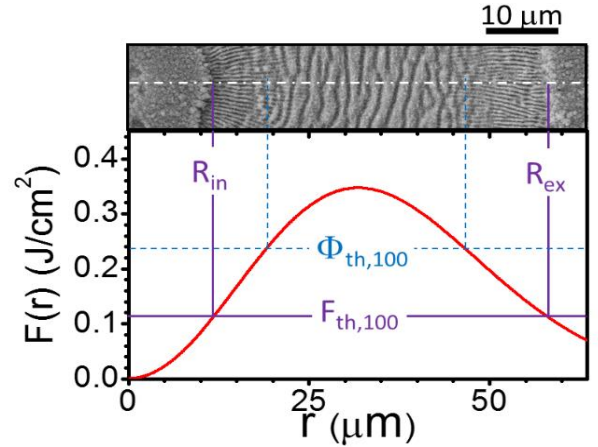


Fig. 5. Zoomed view of a portion of Fig. 2 and the corresponding spatial distribution of the laser pulse fluence illustrating the dependence of the surface texture on the local value fluence. $F_{th,100}$ marks the fluence threshold and the corresponding internal R_{in} and external R_{ex} radii, while $\Phi_{th,100}$ indicates a central region characterized by wrinkles.

Fig. 5 reports a zoomed view of a radial portion of the SEM image of Fig. 2 and the corresponding spatial profile of the laser pulse fluence. It illustrates the close relationship between the surface texture and the local value of the laser fluence. The central area of the annular crater with $F(r) > \Phi_{th,100}$ ($\approx 0.24 \text{ J/cm}^2$) is covered by the wrinkles while the ripples are present in the two low fluence regions with $F_{th,100} < F(r) < \Phi_{th,100}$, where $\Phi_{th,100}$ is the threshold fluence for wrinkles formation at $N=100$. This suggests that: i) appropriate shaping of the fluence profile can be used to fabricate complex surface patterns; ii) an accurate determination of the laser beam parameters (e.g. spot size and peak fluence) can be obtained and correlated with the local laser pulse fluence by means of the structured surface texture; iii) in weak focusing conditions, the two-dimensional vector field structure of intense fs laser beams in a plane orthogonal to the propagation axis can be visualized directly.

Finally, we also analyzed the variation of the internal and external radii with the number of pulses N , for OV beams characterized by azimuthal, radial and circular polarization, at a pulse energy $E_0 \approx 50 \mu\text{J}$. The different polarization patterns were generated by appropriate rotation of the linear polarization of the input beam before the q-plate,

or by using a quarter-waveplate. The results are summarized in Fig. 6. One can observe a progressive rise of the width of the ablated annulus ($R_{\text{ex}}-R_{\text{in}}$) as the number of laser pulses N increases, independently of the specific polarization. The solid curves in Fig. 5 show a model dependence obtained by taking into account the progressive reduction of the fluence threshold due to the incubation effect, and illustrated in the inset for $N=1, 10$, and 100 . The model prediction describes rather well the experimental results.

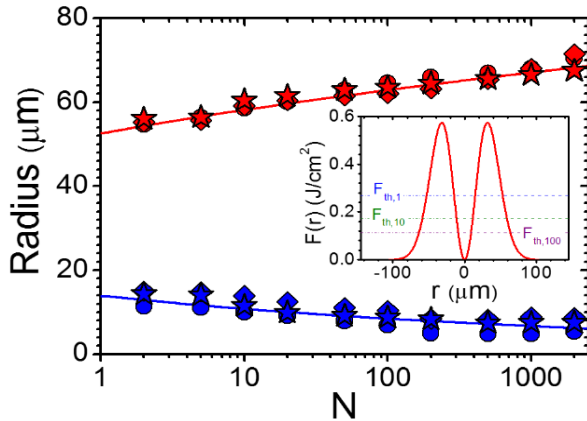


Fig. 6. Variation of the internal (R_{in} , blue data points) and external (R_{ex} , red data points) radii as a function of the number of pulses N for OV beam with azimuthal (circles), radial (diamond) and circular (stars) polarization, at a pulse energy $E_0 \approx 50 \mu\text{J}$. The solid lines are model dependence according to the incubation effect. Inset: OV beam spatial profile and fluence threshold values $F_{\text{th},N}$ for $N=1, 10$, and 100 as predicted by the incubation dependence $F_{\text{th},N} = F_{\text{th},1} \times N^{\xi-1}$, with $F_{\text{th},1} = 0.27 \text{ J/cm}^2$ and $\xi = 0.81$.

Our experimental findings suggest a weak dependence of the threshold fluences for ablation/ripples formation and ripples-to-wrinkles transition on the OV beam polarization, in our experimental conditions. Nonetheless, an earlier report addressed a significant dependence of the ablation efficiency of silicon on the handedness of light for circularly polarized fs OV beams, in tight focusing geometry [13]. This last effect is associated to the generation of a longitudinal electric field component, whose intensity significantly depend on light handedness. In weak focusing conditions, the fraction of beam energy associated to the longitudinal component of the electric field in the focus is negligible. Thus, the OV beam behaves as a 2D vector beam and such an effect disappears, thus explaining the weak dependence observed in our case.

In conclusion, we have carried out an experimental investigation addressing how fs OV beam properties can be determined through the analysis of laser ablation spots. Our experimental findings demonstrate an accurate characterization of intense fs OV beams in weak focusing conditions, as those generally exploited for direct fs laser structuring. Preliminary experiments with OV beams with larger angular momentum confirms the validity of using the imprinted structures as a direct visualization of the polarization pattern in the focal plane. Moreover, the information gathered on the creation of the different surface structures lends itself as a powerful tool for designing specific and well controlled periodic structures on solid targets. Direct fs laser structuring with Gaussian beams is already successfully exploited in the fabrication of functional surfaces, whose characteristics (e.g. optical, wetting, hydrophobic and sensing properties, contaminants or pathogens adhesion, antimicrobial efficacy, etc.) are associated to the peculiar laser produced nano/microstructures (see e.g. Refs. [1] and [26] and papers therein quoted). These generally present a hierarchical form, characterized by larger components (like ripples and wrinkles) decorated with finer, nanoscale structures, which resembles the morphology of natural multifunctional surfaces. The use of fs OV beams is a very young research field that can allow expanding the achievable

geometries of the larger scale features, while retaining the hierarchical structure. This might offer further striking possibilities in tailoring and control of the properties of the surface processed by direct fs laser structuring.

1. A. Y. Vorobyev and C. Guo, *Laser Photonics Rev.* **7**, 385 (2013).
2. T.-H. Her, in *Comprehensive Nanoscience and Technology*, edited by D. Andrews, G. Scholes, and G. Wiederrecht, chapter 4.10 (Elsevier, 2011).
3. S. Amoroso, G. Ausanio, R. Bruzzese, L. Lanotte, P. Scardi, M. Vitiello, and X. Wang, *J. Phys.: Condens. Matter* **18**, L49 (2006).
4. N.N. Nedialkov, P.A. Atanasov, S. Amoroso, R. Bruzzese, X. Wang, *Appl. Surf. Sci.* **253**, 7761 (2007).
5. M. Sanz, M. López-Arias, J. F. Marco, R. de Nalda, S. Amoroso, G. Ausanio, S. Lettieri, R. Bruzzese, X. Wang, and M. Castillejo, *J. Phys. Chem. C* **115**, 3203 (2011).
6. S. Amoroso, S. Tuzi, D.K. Pallotti, C. Aruta, R. Bruzzese, F. Chiarella, R. Fittipaldi, S. Lettieri, P. Maddalena, A. Sambri, A. Vecchione, X. Wang, *Appl. Surf. Sci.* **270**, 307 (2012).
7. M. Liu, *Opt. Lett.* **7**, 196 (1982).
8. J. Bonse, S. Baudach, J. Krüger, W. Kautek, M. Lenzner, *Appl. Phys. A* **74**, 19–25 (2002).
9. M. Duocastella and C. B. Arnold, *Laser Photonics Rev.* **6**, 607 (2012).
10. E. G. Gamaly and A. V. Rode, *Prog. Quant. Electron.* **37**, 215 (2013).
11. Q. Zhan, *Adv. Opt. Photon.* **1**, 1 (2009).
12. C. Hnatovsky, V. G. Shvedov, W. Krolikowski, and A. V. Rode, *Opt. Lett.* **35**, 3417 (2010).
13. C. Hnatovsky, V. G. Shvedov, N. Shostka, A. V. Rode, and W. Krolikowski, *Opt. Lett.* **37**, 226 (2012).
14. O. J. Allegre, Y. Jin, W. Perrie, J. Ouyang, E. Fearon, S. P. Edwardson, and G. Dearden, *Opt. Express* **21**, 21198 (2013).
15. Y. Jin, O. J. Allegre, W. Perrie, K. Abrams, J. Ouyang, E. Fearon, S. P. Edwardson, and G. Dearden, *Opt. Express* **21**, 25333 (2013).
16. K. Lou, S.-X. Qian, X.-L. Wang, Y. Li, B. Gu, C. Tu, and H.-T. Wang, *Opt. Express* **20**, 120 (2012).
17. K. K. Anoop, A. Rubano, R. Fittipaldi, X. Wang, D. Paparo, A. Vecchione, L. Marrucci, R. Bruzzese, and S. Amoroso, *Appl. Phys. Lett.* **104**, 241604 (2014).
18. K. K. Anoop, R. Fittipaldi, A. Rubano, X. Wang, D. Paparo, A. Vecchione, L. Marrucci, R. Bruzzese, and S. Amoroso, *J. Appl. Phys.* **116**, 113102 (2014).
19. C. Hnatovsky, V. Shvedov, W. Krolikowski, and Andrei Rode, *Phys. Rev. Lett.* **106**, 123901 (2011).
20. K. Toyoda, F. Takahashi, S. Takizawa, Y. Tokizane, K. Miyamoto, R. Morita, and T. Omatsu, *Phys. Rev. Lett.* **110**, 143603 (2013).
21. J. Ouyang, W. Perrie, O. J. Allegre, T. Heil, Y. Jin, E. Fearon, D. Eckford, S. P. Edwardson, and G. Dearden, *Opt. Exp.* **23**, 12563 (2015).
22. L. Marrucci, E. Karimi, S. Slussarenko, B. Piccirillo, E. Santamato, E. Nagali, and F. Sciarrino, *J. Opt.* **13**, 064001 (2011).
23. L. Marrucci, C. Manzo, and D. Paparo, *Phys. Rev. Lett.* **96**, 163905 (2006).
24. S. He, J. J. Nivas, K.K. Anoop, A. Vecchione, M. Hu, R. Bruzzese, and S. Amoroso, *Appl. Surf. Sci.* **353**, 1214 (2015).
25. G.D. Tsibidis, C. Fotakis, and E. Stratakis, *Phys. Rev. B* **92**, 041405(R) (2015).
26. A. Y. Vorobyev and C. Guo, *J. Appl. Phys.* **117**, 033103 (2015).

References (full references to aid the reviewer)

- [1] A. Y. Vorobyev and C. Guo, *Direct femtosecond laser surface nano/microstructuring and its applications*, Laser Photonics Rev. **7**, 385 (2013).
- [2] T.-H. Her, *Femtosecond-Laser-Induced Periodic Self-Organized Nanostructures*, in *Comprehensive Nanoscience and Technology*, edited by D. Andrews, G. Scholes, and G. Wiederrecht, chapter 4.10 (Elsevier, 2011).
- [3] S. Amoruso, G. Ausanio, R. Bruzzese, L. Lanotte, P. Scardi, M. Vitiello, and X. Wang, *Synthesis of nanocrystal films via femtosecond laser ablation in vacuum*, J. Phys.: Condens. Matter **18**, L49 (2006).
- [4] N.N. Nedialkov, P.A. Atanasov, S. Amoruso, R. Bruzzese, X. Wang, *Laser ablation of metals by femtosecond pulses: Theoretical and experimental study*, Appl. Surf. Sci. **253**, 7761 (2007).
- [5] M. Sanz, M. López-Arias, J. F. Marco, R. de Nalda, S. Amoruso, G. Ausanio, S. Lettieri, R. Bruzzese, X. Wang, and M. Castillejo, *Ultrafast Laser Ablation and Deposition of Wide Band Gap Semiconductors*, J. Phys. Chem. C **115**, 3203 (2011).
- [6] S. Amoruso, S. Tuzi, D.K. Pallotti, C. Aruta, R. Bruzzese, F. Chiarella, R. Fittipaldi, S. Lettieri, P. Maddalena, A. Sambri, A. Vecchione, X. Wang, *Structural characterization of nanoparticles-assembled titanium dioxide films produced by ultrafast laser ablation and deposition in background oxygen*, Appl. Surf. Sci. **270**, 307 (2012).
- [7] M. Liu, *Simple technique for measurements of pulsed Gaussian-beam spot sizes*, Opt. Lett. **7**, 196 (1982).
- [8] J. Bonse, S. Baudach, J. Krüger, W. Kautek, M. Lenzner, *Femtosecond laser ablation of silicon—modification thresholds and morphology*, Appl. Phys. A **74**, 19–25 (2002).
- [9] M. Duocastella and C. B. Arnold, *Bessel and annular beams for materials processing*, Laser Photonics Rev. **6**, 607 (2012).
- [10] E. G. Gamaly and A. V. Rode, *Physics of ultra-short laser interaction with matter: From phonon excitation to ultimate transformations*, Prog. Quant. Electron. **37**, 215 (2013).
- [11] Q. Zhan, *Cylindrical vector beams: from mathematical concepts to applications*, Adv. Opt. Photon. **1**, 1 (2009).
- [12] C. Hnatovsky, V. G. Shvedov, W. Krolikowski, and A. V. Rode, *Materials processing with a tightly focused femtosecond laser vortex pulse*, Opt. Lett. **35**, 3417 (2010).
- [13] C. Hnatovsky, V. G. Shvedov, N. Shostka, A. V. Rode, and W. Krolikowski, *Polarization-dependent ablation of silicon using tightly focused femtosecond laser vortex pulses*, Opt. Lett. **37**, 226 (2012).
- [14] O. J. Allegre, Y. Jin, W. Perrie, J. Ouyang, E. Fearon, S. P. Edwardson, and G. Dearden, *Complete wavefront and polarization control for ultrashort-pulse laser microprocessing*, Opt. Express **21**, 21198 (2013).
- [15] Y. Jin, O. J. Allegre, W. Perrie, K. Abrams, J. Ouyang, E. Fearon, S. P. Edwardson, and G. Dearden, *Dynamic modulation of spatially structured polarization fields for real-time control of ultrafast laser-material interactions*, Opt. Express **21**, 25333 (2013).
- [16] K. Lou, S.-X. Qian, X.-L. Wang, Y. Li, B. Gu, C. Tu, and H.-T. Wang, *Two-dimensional microstructures induced by femtosecond vector light fields on silicon*, Opt. Express **20**, 120 (2012).
- [17] K. K. Anoop, A. Rubano, R. Fittipaldi, X. Wang, D. Paparo, A. Vecchione, L. Marrucci, R. Bruzzese, and S. Amoruso, *Femtosecond laser surface structuring of silicon using optical vortex beams generated by a q-plate*, Appl. Phys. Lett. **104**, 241604 (2014).
- [18] K. K. Anoop, R. Fittipaldi, A. Rubano, X. Wang, D. Paparo, A. Vecchione, L. Marrucci, R. Bruzzese, and S. Amoruso, *Direct femtosecond laser ablation of copper with an optical vortex beam*, J. Appl. Phys. **116**, 113102 (2014).
- [19] C. Hnatovsky, V. Shvedov, W. Krolikowski, and Andrei Rode, *Revealing Local Field Structure of Focused Ultrashort Pulses*, Phys. Rev. Lett. **106**, 123901 (2011).
- [20] K. Toyoda, F. Takahashi, S. Takizawa, Y. Tokizane, K. Miyamoto, R. Morita, and T. Omatsu, *Transfer of Light Helicity to Nanostructures*, Phys. Rev. Lett. **110**, 143603 (2013).
- [21] J. Ouyang, W. Perrie, O. J. Allegre, T. Heil, Y. Jin, E. Fearon, D. Eckford, S. P. Edwardson, and G. Dearden, *Tailored optical vector fields for ultrashort-pulse laser induced complex surface plasmon structuring*, Opt. Exp. **23**, 12563 (2015).
- [22] L. Marrucci, E. Karimi, S. Slussarenko, B. Piccirillo, E. Santamato, E. Nagali, and F. Sciarrino, *Spin-to-orbital conversion of the angular momentum of light and its classical and quantum applications*, J. Opt. **13**, 064001 (2011).
- [23] L. Marrucci, C. Manzo, and D. Paparo, *Optical Spin-to-Orbital Angular Momentum Conversion in Inhomogeneous Anisotropic Media*, Phys. Rev. Lett. **96**, 163905 (2006).
- [24] S. He, J. J. Nivas, K.K. Anoop, A. Vecchione, M. Hu, R. Bruzzese, and S. Amoruso, *Surface structures induced by ultrashort laser pulses: Formation mechanisms of ripples and grooves*, Appl. Surf. Sci. **353**, 1214 (2015).
- [25] G.D. Tsibidis, C. Fotakis, and E. Stratakis, *From ripples to spikes: A hydrodynamical mechanism to interpret femtosecond laser-induced self-assembled structures*, Phys. Rev. B **92**, 041405(R) (2015).

[26] A. Y. Vorobyev and C. Guo, Multifunctional surfaces produced by femtosecond laser pulses, J. Appl. Phys. **117**, 033103 (2015).